

ABBV-011, A Novel, Calicheamicin-Based Antibody–Drug Conjugate, Targets SEZ6 to Eradicate Small Cell Lung Cancer Tumors



Wolf R. Wiedemeyer, Julia Gavrilyuk, Alexander Schammel, Xi Zhao, Hetal Sarvaiya, Marybeth Pysz, Christine Gu, Monica You, Kumiko Isse, Theodore Sullivan, Dorothy French, Christina Lee, Angeline T. Dang, Zhaomei Zhang, Monette Aujay, Alexander J. Bankovich, and Philip Vitorino

ABSTRACT

In the past year, four antibody–drug conjugates (ADC) were approved, nearly doubling the marketed ADCs in oncology. Among other attributes, successful ADCs optimize targeting antibody, conjugation chemistry, and payload mechanism of action. Here, we describe the development of ABBV-011, a novel SEZ6-targeted, calicheamicin-based ADC for the treatment of small cell lung cancer (SCLC). We engineered a calicheamicin conjugate that lacks the acid-labile hydrazine linker that leads to systemic release of a toxic catabolite. We then screened a patient-derived xenograft library to identify SCLC as a tumor type with enhanced sensitivity to cali-

cheamicin ADCs. Using RNA sequencing (RNA-seq) data from primary and xenograft SCLC samples, we identified seizure-related homolog 6 (SEZ6) as a surface-expressed SCLC target with broad expression in SCLC and minimal normal tissue expression by both RNA-seq and IHC. We developed an antibody targeting SEZ6 that is rapidly internalized upon receptor binding and, when conjugated to the calicheamicin linker drug, drives potent tumor regression *in vitro* and *in vivo*. These preclinical data suggest that ABBV-011 may provide a novel treatment for patients with SCLC and a rationale for ongoing phase I studies (NCT03639194).

Introduction

Calicheamicin, a natural toxin derived from soil dwelling bacterium *Micromonospora echinospora*, is a potent DNA-damaging agent that induces toxicity in many cell types (1, 2). Because of its highly toxic nature, calicheamicin has been leveraged as a payload for antibody–drug conjugates (ADC) in oncology. The first generation of calicheamicin ADCs employed an acid-labile dimethylhydrazine (DMH) calicheamicin linker drug, but its use has been limited to hematologic malignancies, and off-target safety liabilities have required reduced dosing (3). Gemtuzumab ozogamicin (GO), an anti-CD33–directed antibody conjugated to calicheamicin via an acid-labile linker, was the first approved ADC therapy for relapsed/refractory acute myeloid leukemia (AML); however, the acid-labile linker of GO resulted in the systemic release of highly cytotoxic DMH metabolites in patients (3–5). Although GO was approved in 2000, off-target liver toxicity resulted in higher fatality rates compared with standard chemotherapy, and GO was voluntarily withdrawn from the market (6). In 2017, the FDA again approved GO with a modified dosing schedule to reduce toxicities (3). DMH calicheamicin linker drugs were also evaluated for the treatment of

solid tumor types, such as triple-negative breast cancer (TNBC), but no therapeutic window was achieved (7). One significant challenge for solid tumors is reduced drug penetration which requires higher dosing to achieve activity, thereby restricting linker drugs with off-target toxicity profiles (8).

Small cell lung cancer (SCLC) is a high-grade pulmonary tumor type that disproportionately impacts smokers (9). SCLC remains one of the deadliest forms of cancer with a median survival of less than 10 months for patients with advanced disease, due in part to low durability of existing therapies (10). SCLC is a neuroendocrine (NE) tumor type which is characterized by high expression of ASCL1, a transcription factor that drives NE cell fate (11). Consequently, NE markers, including chromogranin A (CHGA) and SYP, are highly expressed and used as diagnostic markers for the disease (12). The restricted expression of NE markers makes them desirable candidates for targeted drug delivery; however, neither SYP nor CHGA are expressed on the cell surface (13).

Here we describe the development of ABBV-011, a novel SEZ6-targeted ADC for the treatment of SCLC. ABBV-011 is conjugated to a novel calicheamicin linker drug, LD19.10, that lacks the acid-labile DMH found in previous calicheamicin ADCs. Antibody conjugates of LD19.10 produce charged catabolites that are markedly less cytotoxic than the DMH catabolites detected in ADCs with acid-labile calicheamicin linkers. In a cross-indication patient-derived xenograft (PDX) screen, we found that SCLC tumors are highly sensitive to an LD19.10-based ADC. Using a bioinformatic approach, we identified seizure-related homolog 6 (SEZ6) as a novel SCLC ADC target. By mRNA expression analysis and IHC, SEZ6 is a highly expressed surface marker in SCLC with limited expression in normal tissue. We used a murine hybridoma screen to identify SC17, a SEZ6 binding antibody that induces rapid receptor internalization. ABBV-011, which is comprised of SC17 conjugated to LD19.10, combines a novel targeting approach and linker drug to selectively kill SCLC tumors expressing SEZ6 *in vitro* and *in vivo*.

AbbVie Inc., North Chicago, Illinois.

Note: Supplementary data for this article are available at Molecular Cancer Therapeutics Online (<http://mct.aacrjournals.org/>).

Corresponding Author: Philip Vitorino, Bristol-Myers Squibb (United States), Redwood City, CA 94603. Phone: 650-380-5513; E-mail: pvitorino@gmail.com

Mol Cancer Ther 2022;21:986–98

doi: 10.1158/1535-7163.MCT-21-0851

This open access article is distributed under Creative Commons Attribution-NonCommercial-NoDerivatives License 4.0 International (CC BY-NC-ND).

©2022 The Authors; Published by the American Association for Cancer Research

Materials and Methods

Lysosomal stability test

ABBV-011 was prepared in 50 mmol/L ammonium acetate (pH 5) at the concentration of 10 µg/mL in the presence of 0.25 mg/mL of human liver lysosomes (Xenotech LLC). They were incubated at six different timepoints (0, 1, 2, 4, 24, and 48 hours). The reaction was terminated by acetonitrile containing internal standard. Following centrifugation, the test compounds were dried under N₂. The samples were then dissolved in ACN/H₂O (50/50) for LC/MS analysis.

The analytes were separated on a 2.1 × 50 mm Luna Omega Polar C18 column (1.6 µm in particle size). The composition of mobile phase A was 0.1% formic acid in water and that of mobile phase B was 0.1% formic acid in acetonitrile, respectively. The gradient program was: 0 minute, 5% B; 1 minute, 5% B; 15 minutes, 95% B; 16 minutes, 95% B; 16.1 minutes, 5% B; 20 minutes, 5% B. The flow rate was 0.4 mL/minute and the column temperature was set at 50°C. The injection volume was 20 µL. The subsequent mass spectrometry (MS) analysis was done on a Thermo Fisher Scientific Orbitrap MS operated in positive ion electrospray ionization (ESI) mode. Data were acquired in the full scan mode from m/z of 150 to 1,500 at the resolution of 120,000, followed by most intense ion MS/MS and MS/MS data-dependent scans at the resolution of 15,000.

S9 incubation test

ABBV-011 was incubated at 1 mg/mL with rat and human liver S9 fraction with the addition of UDPGA, glutathione (GSH), and corresponding cofactors at 37°C for 1 and 48 hours. The reaction was terminated by acetonitrile containing internal standard. Following centrifugation, the test compounds were dried under N₂. The samples were then dissolved in ACN/H₂O (50/50) for LC/MS analysis. The LC/MS condition was same as described in lysosomal stability test.

IHC

Formalin-fixed paraffin-embedded (FFPE) blocks were sectioned on a microtome at 4 µm thickness and dried for 2 hours prior to baking at 65°C for 20 minutes. Deparaffinization, rehydration, and target retrieval were performed using a 3-in-1 procedure on the Dako Autostainer platform. Prior to antibody staining, samples were blocked with the Envision FLEX Peroxidase blocking reagent for 5 minutes. The SEZ6 IHC antibody was developed through an internal immunization campaign and was used at 4.0 µg/mL for 30 minutes to stain tissue slides. After washing, EnVision FLEX HRP was used to visualize sample. EnVision FLEX diaminobenzidine (DAB+) was used as substrate for chromogen formation. Before final rinse, sections were stained with hematoxylin followed by a final rinse. After final rinse, slides were dehydrated in alcohol, cleared in xylene, and mounted with glass coverslips with mounting media. Staining was scored by a pathologist using visual inspection for staining prevalence and intensity. Positive versus negative SEZ6 IHC staining of the normal tissues was determined using a microscope objective ≤ 20×. Normal cell staining with the SEZ6 IHC assay was considered positive if any intensity of the DAB signal was present. The IHC staining pattern in normal cells was considered positive if cytoplasmic and/or membranous staining was present.

Human SCLC FFPE samples were procured from Discovery Life Sciences which Clinical Laboratory Improvement Amendments–certified labs, stringent Institutional Review Board and Ethics Committee compliance, and all of the applicable regulations, guidelines, and best practices that meet or exceed the U.S. and international

regulatory requirements, including the EU's GDPR. Written informed consent was obtained from all patients who supplied samples for this study.

Western blotting analysis

Cells were lysed in Pierce immunoprecipitation lysis buffer with protease inhibitor cocktail. Protein samples (40 µg) and Magic protein marker were run on Thermo Fisher Scientific Xcell SureLock mini gels in 1×MOPS buffer. After transfer to polyvinylidene difluoride membrane with iBlot, blots were blocked with 5% milk in TBST. Primary Ab (from internal campaign, 5 µg/mL) was added in block buffer for overnight shaking at 4°C. After three 10-minute washes in TBST, 1:5,000 dilution of secondary antibody (Jackson Immuno Research, 715-035-150) in block reagent was added for 1 hour at room temperature. After final washes, SuperSignal West Femto was used for LI-COR detection of protein bands.

Transcriptomics profiling

Affymetrix (Thermo Fisher Scientific Inc.) Clariom D human microarray platform was used to generate transcriptomics survey across a range of tissue types in the PDX bank. Raw data were GC content corrected using Affymetrix power tools. Robust multi-array average (RMA) normalization (14) was performed on GC-corrected cell files across all tumor samples and normal samples that passed quality control. Expression values were log₂ transformed.

RNA sequencing (RNA-seq) was performed with mRNA extracted from fresh-frozen PDX tumor tissue samples. cDNA libraries were prepared from poly(A) selected RNA applying the Illumina TruSeq protocol for mRNA. The libraries were then sequenced on Illumina HiSeq 2000 instrument (Illumina) to generate 150 bp paired-end reads with a sequencing depth of 50M reads per sample. FASTQ files were processed using OmicSoft RNA-seq pipeline with HG38 annotation. TPM values were calculated as gene level quantifications, and were further log₂ transformed.

Genome-wide association with CHGA

Pairwise Pearson correlation coefficients between CHGA and all cell surface markers were computed using RNA-seq data of the PDX SCLC samples, as well as within individual human SCLC cohorts (15–17). Furthermore, the set of correlation coefficients from human studies for each gene pair were combined into a single meta correlation coefficient using Fisher Z-transformation.

Molecular subtyping

Samples were assigned to the subtype classes based on highest expresser among the four transcriptional factors, ASCL1 (SCLC-A), NEUROD1 (SCLC-N), POU2F3 (SCLC-P), and YAP1 (SCLC-Y).

Survival analysis

Overall survival was used as clinical endpoint. Follow-up time was defined as time from diagnosis until death, or time of last follow-up if the outcome of patient was not known. Three published human SCLC cohorts were included (15–17). The median value of the target expression within each study was used as cutoff to assign patients into high or low expression groups within each cohort. Survival probabilities associated with the expression groups were shown by the Kaplan–Meier curves, and the corresponding log-rank *P* values were reported.

All analysis was carried out in R statistical environment (18), unless otherwise specified.

Flow cytometry

Antibodies were conjugated to the fluorophore Alexa Fluor647 (A647) or PE using standard methodology. Cell lines growing in culture were collected in Hanks Balanced Salt Solution (HBSS) supplemented with 2% FBS and 13mM 1 mol/L HEPES buffer per 500 mL HBSS (FSM buffer), filtered through 100 and 40 μ m cell strainers, and stained with 1 μ g of conjugate antibody per 10^6 cells for 20 minutes on ice. Cells were washed twice in FSM and analyzed on a BD Aria III cytometer. Established xenograft tumors were dissociated and subjected to a mild enzymatic digestion step that preserved cell surface epitopes. Single-cell suspensions were then stained with an antibody cocktail to distinguish populations within the human tumor cell compartment (human ESA positive/mouse lineage negative cells).

Antibody internalization

A549 cells were transfected with an in-house lentivector (pLMP-hLAMP1-CmRuby2) to express LAMP1, a lysosomal membrane glycoprotein fused to mRUBY. Cells were then transduced to express SEZ6. Cells were cultured in a T75 flask to approximately 80% confluency and harvested with trypsin into a single-cell suspension. A total of 5,000 cells per well were seeded in tissue culture plates at 50 mL/well culture media and incubated at 37°C for 24–48 hours. Cells were stained with NucBlue, a cell permeant nuclear counterstain that emits blue fluorescence, for 20 minutes at 20°C–25°C (two drops/1 mL diluted in FSM). After three wash steps, the cells were stained with SC17 or human IgG isotype antibody reagents for 1 hour on ice at 10 mg/mL. Following primary antibody, the cells were washed three times and stained with a secondary antibody (Alexa-647 Goat Anti-human) at 10 mg/mL for 30 minutes on ice. Plates were imaged with to view the lysosome in the TRITC channel (lysosome), target SEZ6 in the APC channel, and the nucleus in the PacBlue channel on the Cell Insight CX5 automated epifluorescent microscope (Thermo Fisher Scientific) within a 10-minute time period to obtain a time zero image. For each culture condition, two technical replicate wells were set up and analyzed independently. After imaging, one plate was kept strictly at 4°C for 4 hours while the second plate was incubated at 37°C in an incubator with 5% CO₂. Following incubation, plates were imaged to obtain a postincubation image to look for internalization. Images were analyzed for each fluorescent color separately and composite images assembled in a second step to visualize fluorescent colocalization.

In vitro cellular toxicity assays

HEK293T cells with or without SEZ6 overexpression were plated at 500 cells per well in a 96-well plate. Antibodies were added at 50 pmol/L before addition of Fab saporin at a final concentration of 2 nmol/L. Cells were incubated for 96 hours. Cell titer glo was used to assess viable cells based on manufacturer's protocol. For ADC killing assays, cells were plated at 500 cells per well. ADC was added as a 1:5 dose titration from 100 to 0.001 nmol/L. After 96 hours, cell viability was assessed using Cell Titer Glo according to manufacturer instructions. All cell lines were obtained from ATCC and did not exceed six passages. Cells were thawed for at least 2–3 days prior to use in experiments. No additional cell authenticity analysis was run. *Mycoplasma* testing was run upon generation of frozen stocks or prior *in vivo* implantation."

In vivo pharmacokinetics of ABBV-011 in immunocompromised mice

All *in vivo* studies were conducted in female NOD/SCID mice (5 to 10 weeks of age; Charles River Laboratories), in accordance with protocols approved by the AbbVie Stemcentrx Institutional Animal Care and Use Committee. Animal health was monitored daily, and

humane euthanasia was performed at protocol clinical endpoints per the American Association for Laboratory Animal Science guidelines.

Single intravenous dose pharmacokinetics of ABBV-011 was assessed in naïve (non-tumor-bearing) NOD/SCID mice at 0.5, 1, 2, 4, 6, and 8 mg/kg. ABBV-011 was coadministered with 10 mg/kg HuIgG1 naked antibody to minimize Fc γ R macrophage sink effects and be consistent with dosing approaches used in efficacy studies (see below). Whole blood was collected from individual mice using submandibular or tail vein collection techniques at 0.083 (5 minutes), 4, 24, 72, 96, 120, 168, 216, 336, 504, and 624 hours post-ABBV-011 dosing. Whole blood volumes (100 μ L volume) did not exceed Institutional Animal Care and Use Committee protocol limits (19), and mice received fluid replacement (0.9% saline, subcutaneous administration) to aid in recovery from blood sampling. Whole blood was processed to serum via centrifugation at 12,100 \times g for 5 minutes at room temperature and stored at –80°C until bioanalysis of ADC concentrations was performed.

ADC levels in mouse serum were measured using an ELISA-based assay with electrochemiluminescent detection [mesoscale discovery (MSD); S600 imager] of calicheamicin-conjugated ADC. Briefly, capture antibody (an internally made anti-calicheamicin warhead antibody) was bound to MSD plates, followed by serum sample incubation, and finally, detection with goat anti-human IgG, Fc γ fragment specific sulfotagged antibody. MSD plates were washed with 0.05% volume/volume Tween 20 in PBS in between incubation steps. After chemiluminescent signals were read, serum concentrations (average of two replicates) were extrapolated from a linear standard curve. ADC serum concentrations (log scale) were plotted versus time since dose administration.

In vivo efficacy of ABBV-011 in SCLC PDX mouse models

SCLC PDX models were previously established from patient biopsies (20) and passaged in NOD/SCID mice no more than five times to expand tumor cells to implant for efficacy studies. Tumors were excised and cells were dissociated as single-cell suspensions to implant 50,000 PDX tumor cells as a subcutaneous tumor near the mammary fat pad. Once tumors grew in range between 90 and 300 mm³ volume (average volume: 140–200 mm³), mice were randomized into groups of 5 to 8 mice per group for treatment. Mice were tested with the following treatments: (i) vehicle [5% glucose/saline, saline, or 15 mmol/L Histidine + 7.5% (w/v) sucrose pH6.0 buffer] (ii); ABBV-011 ADC (SC17-LD19.10) at 0.5, 1, 2, 4, and/or 8 mg/kg (iii); non-targeted control ADC (HuIgG1-LD19.10) at 1, 2, 4, and/or 8 mg/kg (iv); positive control anti-human CD46 ADC (CD46-LD19.10) at 1, 2, 4, or 8 mg/kg; and/or (v) a single cycle of pharmaceutical-grade cisplatin + etoposide chemotherapy. All compounds were administered intraperitoneally, and ADCs or vehicle were administered as a single dose. Cisplatin etoposide chemotherapy was administered as a single dose of 5 mg/kg cisplatin and three daily doses of 8 mg/kg etoposide; on day one, administration of cisplatin and etoposide were staggered by at least 4 hours to enable absorption of individual compounds before mixing. Animals treated with ADC received a coadministration of 10 mg/kg HuIgG1 naked antibody to increase the exposure and diminish effects of the Fc γ R macrophage sink inherent to immunocompromised mice. Animal body weights and tumors were measured at least once weekly using an electronic scale and caliper, respectively. Tumor volume was calculated as the volume of a prolate ellipsoid, based on measurements (in millimeters) along a long and short axis: $0.5 \times \text{long axis} \times \text{short axis} \times \text{short axis}$. Animals were humanely euthanized if body weight measurement reached \geq 20% weight loss; when individual tumor volume

measurements reached $\geq 1,000 \text{ mm}^3$, or group average tumor volume measurements $\geq 800 \text{ mm}^3$; if animals had poor physiologic condition per protocol guidelines; or, if the study reached 150 days postinitial dose administration.

Blood samples were taken 24 hours posttreatment of ADCs to confirm expected dose levels received in individual mice using the same blood sampling and bioanalysis methods described above (see Pharmacokinetics study section). Any mouse exhibiting ADC concentrations $\pm 50\%$ of the average expected concentration, calculated as the dose \times mouse body weight/2 mL blood volume, were excluded from efficacy analyses.

In vivo efficacy was determined by graphing the tumor volume versus time, and the percent tumor growth inhibition (%TGI) and time to tumor progression (TTP) were calculated from the graph. The %TGI was calculated as follows: (i) the timepoint at which the first vehicle-treated reached $1,000 \text{ mm}^3$ was recorded; (ii) the average tumor volume of vehicle-treated mice at the timepoint (step 1) was recorded; (iii) for each individual mouse on study, the ratio of the volume at the timepoint (step 1) divided by the average vehicle volume (step 2); and (iv) the median of all mice in treatment group was calculated as the treatment group %TGI. Negative %TGI values were updated to 0. TTP (units: days) was first calculated for each individual mouse as the duration (in days) since treatment, when tumor volumes reached at least 100 mm^3 greater than the nadir (minimum) tumor volume, and, then the median of individual mouse TTPs within a treatment group was calculated as the treatment group TTP. To account for broader types of responses in different cancer subtypes and tumor growth characteristics, TTP evaluation for tumor responses to either anti-CD46-LD19.10 or anti-CD46-PBD (pyrrolobenzodiazepene) were calculated as the timepoint to when tumor volumes reached at least twice the size of the tumor volume at treatment group randomization. For delayed or static responses, the nadir was recorded as the minimum volume following initial growth phase or as the volume at stasis, respectively. For durable responses, the study duration till mouse euthanasia was recorded as the TTP, and a ">" is inserted in front of the value for groups when more than 50% of individual mice in the group had durable responses. Mice that were euthanized before the study reached 50 days duration postinitial treatment, and whose TTP could not be calculated per above criteria, were excluded from analyses.

Synthesis and conjugation of LD19.10

Synthesis of LD19.10 and its conjugation are described in full detail in WO2019232241 (21). In brief, the key step of the LD19.10 synthesis links together maleimide-PEG-amine 1 with N-Acetyl calicheamicin-derived carboxylic acid 2 in the presence of COMU coupling reagent and *N,N*-diisopropyl ethylamine in dimethylformamide (DMF; Supplementary Fig. S1A). The product linker-drug LD19.10 is isolated by reverse phase HPLC and stored frozen and protected from light. Anti-SEZ6 antibody (SC17), anti-CD46 antibody, or HuIgG containing two site-specifically engineered cysteines is prepared for conjugation by subjecting it to mild reduction in a buffer containing L-arginine/EDTA with a predetermined concentration of reduced GSH pH8.0 for 20 hours. The antibody is then exchanged into Tris/EDTA buffer pH7.0 and conjugated to LD19.10 for 1 hour (Supplementary Fig. S1A). The pH is then adjusted to pH6.0 and the ADC is buffer exchanged by diafiltration into the formulation buffer containing sucrose and polysorbate-20. The ADC has been analyzed by RP-HPLC for drug-to-antibody ratio (DAR) of 2.0, SEC for aggregation and *in vitro* cytotoxicity for activity. All material used (mAb and ADC) had

>99% monomer peak by SEC (e.g., less than 1% high molecular weight [HMW] and fragments).

SC17 sequence information

SC17 sequence and purification methods are summarized in US20210338831 (22). The sequence of SC17 is also available through Chemical Abstract Service (registry number 2642063-73-6).

Data availability statement

RNA-seq datasets used to evaluate gene expression in SCLC human samples were obtained from Gene Expression Omnibus at GSE60052, from ArrayExpress at accession number E-MTAB-1999, and from European Genome-Phenome Archive under accession code EGAS00001000925. Other data generated in this study are available within the article and its Supplementary Data.

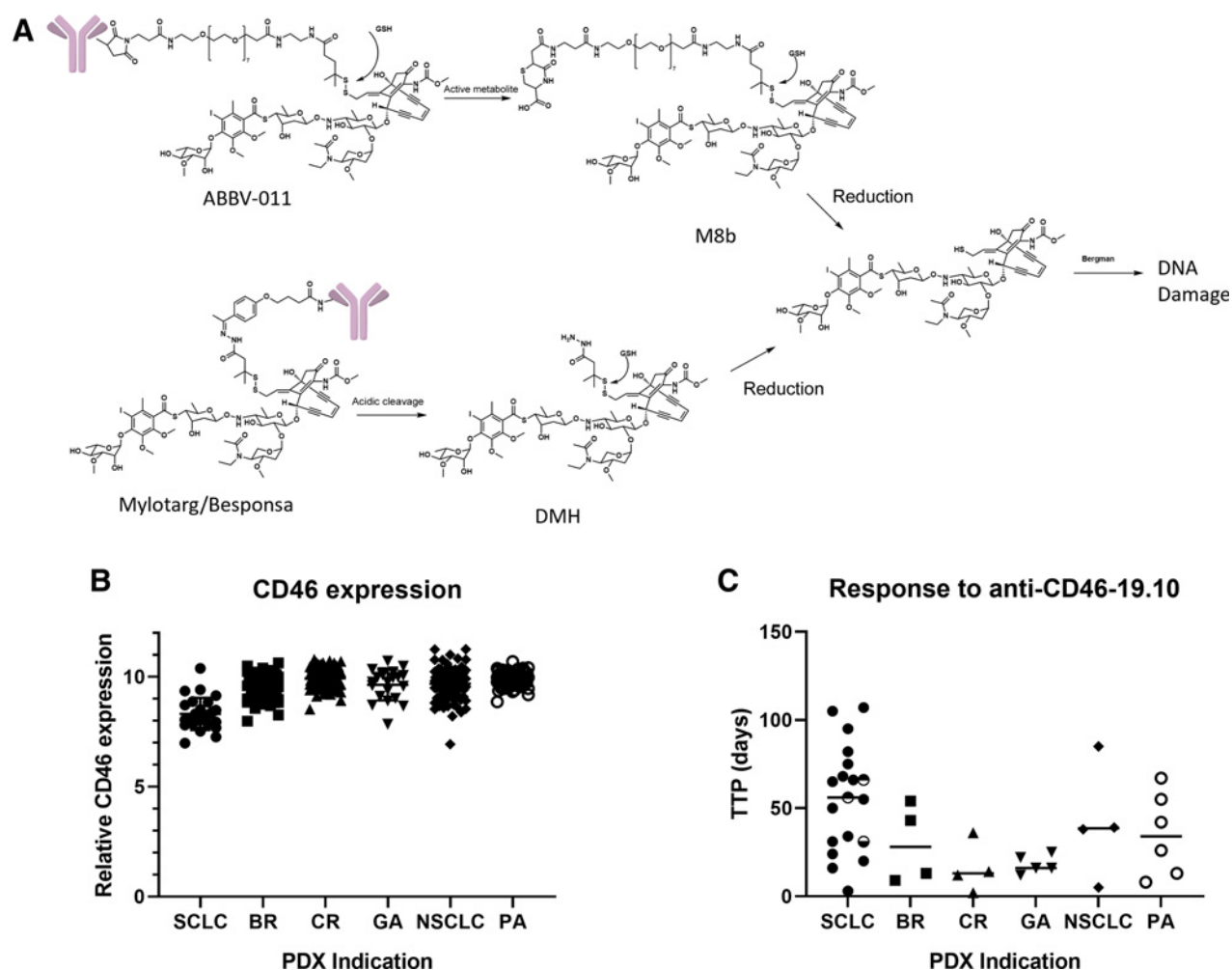
Results

Modified linker chemistry in LD19.10 eliminates toxic DMH catabolite from acid-labile calicheamicin linker drug

Acid-labile calicheamicin-based linker drugs have been conjugated to mAbs targeting tumor-associated receptors such as CD33 in AML and CD22 in ALL (23, 24). While inotuzumab ozogamicin (Besponsa; anti-CD33) and gemtuzumab ozogamicin (Mylotarg; GO, anti-CD22) are approved therapies in hematologic malignancies, these ADCs are associated with clinical adverse events such as infection, thrombocytopenia, febrile neutropenia, leukopenia, and more rarely, veno-occlusive disease (23, 24). The acid labile linkers used by GO are designed to cleave in the acidic environment of the lysosome, but previous reports have shown that the DMH catabolites of GO can be detected in circulation and can potentially induce cell toxicity (4). To mitigate liabilities associated with free DMH catabolites, we engineered a calicheamicin linker drug that lacks the acid labile hydrazone group (LD19.10; Fig. 1A). Instead of relying on acid hydrolysis, LD19.10 dissociates only upon reduction of the hindered disulfide before or after antibody degradation (Fig. 1A).

To determine the catabolic products of LD19.10, we conjugated the linker drug to SC17, a mAb directed against SEZ6. To model catabolic products *ex vivo*, the ADC was incubated with lysosomal and microsomal preparation to mimic catabolism from target-mediated and liver uptake, respectively. In addition, the ADC was injected into rats and cynomolgus monkeys to understand the catabolite profiles *in vivo*. MS analysis of the microsomal preparations (S9 incubation) showed no detectable catabolites except for the Bergman product, N-acetyl-calicheamicin, the nontoxic product of calicheamicin catabolism (1). This suggested that the LD19.10 ADC is not significantly degraded within the liver compartment. Combined mass spectrometry analysis from the lysosomal preparations and animal serum revealed a single metabolic product that can rearrange into a linear (M8a) or cyclic (M8b) form (Fig. 1A; Supplementary Fig. S1B). While M8a could be detected in acidic lysosomal preparations, only M8b was detected in the more basic environment of rodent and primate plasma, suggesting that the rearrangement is pH dependent (Supplementary Fig. S1C).

DMH catabolites of calicheamicin have been shown to potentially kill cells with a cellular IC_{50} of 5.1 nmol/L (Table 1; ref. 4). Although LD19.10 eliminates the DMH catabolite, we wanted to assess whether the M8a or M8b catabolites could contribute to cellular toxicity. M8a and M8b lack the amine groups in DMH and contain a charged carboxylic acid group (Fig. 1A), suggesting that they would exhibit poor membrane permeability. Consistent with this hypothesis, the M8a and M8b

**Figure 1.**

A, Modified linker drug chemistry in LD19.10 to eliminate toxic DMZ catabolite from calicheamicin linker drug. Chemical structure and metabolic pathway for the 19.10 linker drug in ABBV-011 compared with the acid-labile linker drug used in clinically approved calicheamicin-based ADCs. **B**, RNA expression of ubiquitously expressed surface antigen CD46 across PDX of varying indications by microarray analysis. **C**, PDX tumor response to a single dose of anti-CD46 antibody conjugated to LD19.10 calicheamicin linker drug in murine tumor models derived from multiple tumor indications. Animals were dosed with 2 (SCLC PDX top half-filled circles), 4 (SCLC PDX filled circles), or 8 mg/kg (all others) as indicated.

catabolites induced cellular toxicity with an IC_{50} of 1,400 and 1,200 nmol/L, respectively, more than 200-fold less potent than DMH (Table 1).

Although DMH catabolites of acid labile linkers could contribute to toxicity, these linker drugs achieved a positive therapeutic index in hematologic cancers. In solid tumors, the higher dosing required to overcome challenges with intratumoral drug delivery could limit the

Table 1. Catabolite profiles for ABBV-011 versus Mylotarg.

Catabolite (drug)	<i>In vitro</i> potency (nmol/L)	Detectable in plasma?
DMH (Mylotarg)	5.1	Yes
M8a (ABBV-011)	1,400	ND
M8b (ABBV-011)	1,200	Yes

Note: Potency of calicheamicin drug metabolites DMH, M8a, and M8b in cell-killing assays (middle column). The detectability of metabolites in primate plasma is listed after dosing with corresponding ADC (right column).

therapeutic index (25). Because LD19.10 does not contain DMH catabolites, we wanted to explore whether an ADC conjugated to LD19.10 could achieve responses in a solid tumor setting. To assess the potential for an LD19.10-based ADC, we conjugated LD19.10 to an antibody specific for CD46, a widely expressed tumor antigen (26), and tested ADC activity across a panel of PDX representing different tumor indications. To confirm that CD46 was broadly expressed, we generated microarray data to evaluate CD46 in a panel containing SCLC, TNBC, estrogen receptor-positive (ER^+) breast cancer, colorectal cancer, gastric cancer, non-small cell lung cancer (NSCLC), and pancreatic cancer PDX tumors. The expression of CD46 was uniformly high in all tumor types tested with a slightly lower expression observed in SCLC (Fig. 1B). We then profiled the anti-CD46-LD19.10 ADC and compared response with a nontargeting IgG1-LD19.10, using TTP following treatment as a readout (Fig. 1C). The 8 mg/kg dose of CD46-LD19.10 ADC induced modest antitumor activity across most indications other than SCLC, but a 2–4 mg/kg dose resulted in robust antitumor activity in SCLC, despite lower CD46 expression

(Fig. 1C). To confirm that the CD46 antigen was capable of inducing internalization of the LD19.10 ADC, we also profiled a CD46-directed antibody conjugated to a potent PBD warhead. Unlike the LD19.10 payload, the anti-CD46-PBD ADC potently inhibited tumor growth across all indications tested (Supplementary Fig. S1D). These data suggest that SCLC is a solid tumor indication uniquely sensitive to the LD19.10 linker drug.

SEZ6 transcript is expressed in NE SCLC with minimal expression in normal tissues

Given the increased sensitivity of SCLC to the LD19.10 linker drug (Fig. 1C), we sought to identify a target that efficiently and selectively delivers the LD19.10 warhead in SCLC tumor cells. While NE markers such as CHGA are known to be highly expressed and restricted to SCLC and NE cells, these antigens are not expressed on the cell surface limiting their potential as ADC targets. To identify a NE ADC target for SCLC, we employed a genome-wide bioinformatic survey of genes coding for membrane-associated proteins to identify surface receptors whose expression most closely correlate with CHGA, a bona fide diagnostic marker for SCLC. Figure 2A summarizes the correlation coefficient between each membrane-associated protein transcript and CHGA across 66 SCLC PDX RNA-seq samples (y-axis) and 188 primary SCLC samples combined across three human SCLC cohorts (refs. 15–17; x-axis). The transcripts most correlated to CHGA were similar between the primary and PDX samples (Fig. 2A), supporting robust coregulation. SEZ6, a single pass transmembrane receptor, was among the top CHGA correlates with R-squared values of 0.77 and 0.76 in the PDX and primary SCLC samples, respectively (Supplementary Fig. S2A). When we surveyed SEZ6 expression by microarray

across a panel of PDX samples spanning multiple solid and heme tumor indications, we found SEZ6 was highly and uniquely expressed in NE cancers including SCLC, large cell NE cancer and small cell cancer of the ovary (Fig. 2B; refs. 27, 28). RNA-seq analysis of a larger set of SCLC PDX confirmed the robust expression in SCLC as compared with other indications (Supplementary Fig. S2B). We selected SEZ6 as a lead candidate for ADC development given its high expression in SCLC and its published role in neuronal and NE cell types (29–31).

To achieve a therapeutic index clinically, ADC targets must be highly expressed in tumors but also minimally expressed in normal tissues. By microarray and RNA-seq, low SEZ6 expression was observed in normal tissues such as trachea, heart, stomach, skin, muscle, esophagus, pancreas, skin, lung, kidney, large intestine, liver, small intestine (Fig. 2B, left; Supplementary Fig. S2B). Consistent with our data, the GTEx normal tissue expression database indicates minimal SEZ6 expression across most normal tissues with elevated SEZ6 expression restricted to neural or NE tissues such as brain and pituitary gland (Supplementary Fig. S2C). Low SEZ6 expression was also observed in heavily innervated tissues like colon and adrenal gland (Supplementary Fig. S2C). Though detectable, the SEZ6 expression observed in normal tissues was significantly lower than the levels of SEZ6 detected in the corresponding SCLC PDX samples (Fig. 2B; Supplementary Fig. S2B). To further explore the cancer-dependent upregulation of SEZ6 in human tissues, we used previously published RNA-seq data from primary SCLC tumors (15) to compare the expression of SEZ6 between tumor cells (n = 79) and healthy human lung (n = 7). SEZ6 expression was significantly upregulated in SCLC tumor cells as compared with normal lung (Fig. 2C). Taken together,

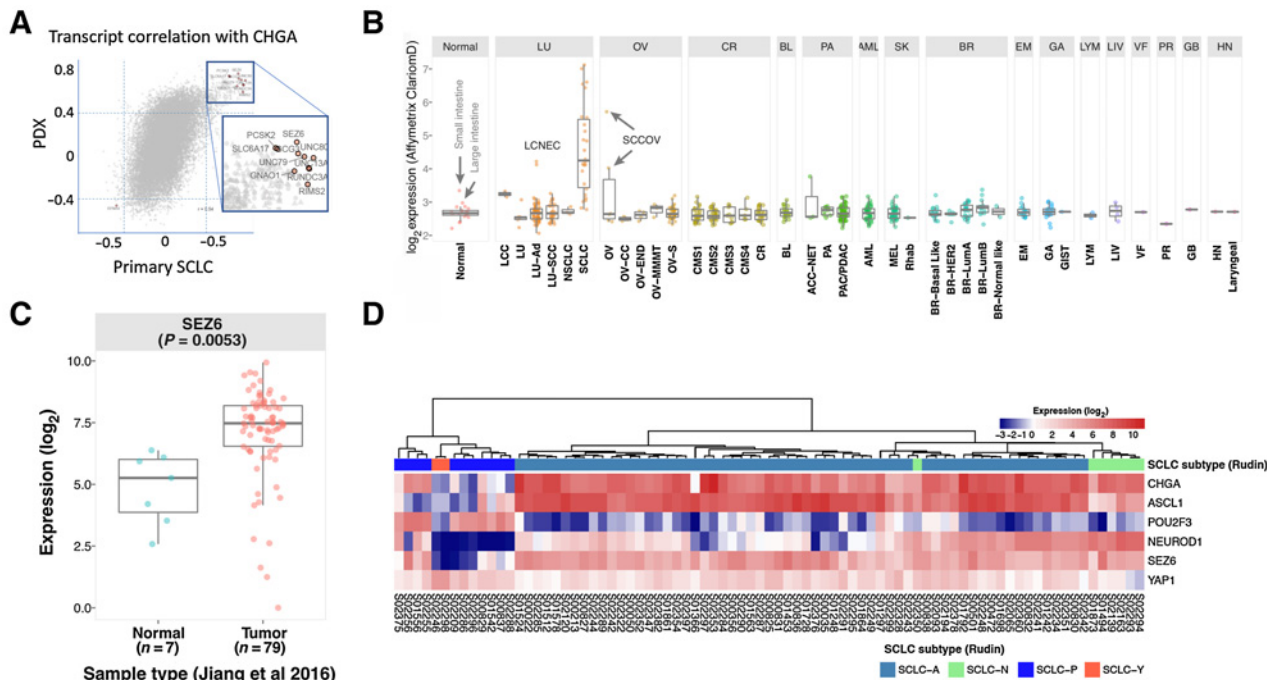


Figure 2. SEZ6 is expressed in NE SCLC with minimal expression in normal tissues. **A**, Comparison of pairwise Pearson correlation between CHGA and all cell surface markers in PDX setting (y-axis) and in human primary setting combined across three published human cohorts (refs. 15–17; x-axis). **B**, Microarray data (Affymetrix Clariom D platform) of PDX shows SEZ6 expression is high in SCLC PDX, but low in normal tissues and other cancers. **C**, SEZ6 had upregulated expression in human SCLC tumors (n = 79) compared with the normal reference (n = 7) from the SCLC79 cohort (16). **D**, Hierarchical clustering with Euclidean distance and Ward linkage on expression of genes of interest in the Ucologne cohort (15).

these data suggest SEZ6 expression is elevated in SCLC as compared with normal tissues.

SCLC has been recently classified into four distinct molecular subtypes based on the expression of key transcription factors including ASCL1, NEUROD1, POU2F3, and YAP (32). To understand the expression of SEZ6 in the context of molecular subtypes, we ran hierarchical clustering of published RNA-seq data for key transcription factors and classified each sample into one of four reported subtypes (SCLC-A, SCLC-N, SCLC-P, and SCLC-Y, **Fig. 2D**). Consistent with the previous transcription data, SEZ6 and CHGA expression are correlated (**Fig. 2A and D**). SEZ6 is highly expressed throughout all ASCL1-high tumors in the SCLC-N and SCLC-A subtypes but has lower expression in the ASCL1-low/POU2F3-high SCLC-P and SCLC-Y subtypes (**Fig. 2D**; Supplementary Fig. S2D, left). In addition, SEZ6 RNA expression is significantly elevated in advanced stages of SCLC (ref. 15; Supplementary Fig. S2D, right).

To understand whether SEZ6 expression can impact clinical outcome in patients with SCLC, we compiled patient outcome data from three separate SCLC RNA-seq studies representing a total of 188 patients (15–17). Survival outcomes were significantly worse for patients with SEZ6 tumor expression above the median as compared with patients with SEZ6 expression below the median value (Supplementary Fig. S2E). The poor outcome for patients with high SEZ6 supports ADC development to target antigen-positive cells, but more data is needed to understand whether SEZ6 plays any functional role in SCLC development or survival.

SEZ6 is a prevalent cell surface protein target in SCLC with minimal normal tissue expression

RNA expression supports SEZ6 as a promising ADC target in SCLC, so we assessed whether SEZ6 protein could be detected in normal and tumor tissues. To do this, we screened a large panel of internally generated antibodies for selective SEZ6 staining, defined by the ability to detect SEZ6 in endogenous and overexpressing cell lines but not in corresponding knock out cells (Supplementary Fig. S3A and S3B). Similar to Western blot results, SEZ6 IHC signal was strong in 293T cells overexpressing SEZ6 and in NCI-H69, a SCLC cell line with endogenous SEZ6 expression; however, no IHC signal was seen in 293T parental cells or in NCI-H69 with CRISPR-mediated knockout (KO) of the SEZ6 locus (Supplementary Fig. S3A and S3B). Next, we confirmed IHC assay sensitivity by evaluating SEZ6 staining in a panel of SCLC cell lines with a range of endogenous SEZ6 expression by Western (Supplementary Fig. S3C and S3D). Protein quantification by densitometry (Western) and H-score (IHC) indicated an R-squared correlation value of 0.72 between the orthogonal protein detection methods, suggesting that the IHC assay is both sensitive and selective (Supplementary Fig. S3C–S3E).

The validated IHC assay was used to stain SEZ6 in SCLC PDX and primary samples. In PDX, SEZ6 protein expression was robustly detected and the signal intensity was consistent with SEZ6 mRNA expression in the samples (Supplementary Fig. S3F). In positive PDX tumors, IHC staining for SEZ6 was strong and detectable in the plasma membrane and cytoplasm with most abundance staining at the cell surface, consistent with previous reports of SEZ6 plasma membrane expression in neuronal cells (Supplementary Fig. S3F; ref. 33). In primary SCLC samples, SEZ6 IHC staining exhibited a range of positivity from no detectable signal to near saturated signal across the tumor (**Fig. 3A**). Similar to PDX, expression was detected on the cell surface and in the cytoplasm (**Fig. 3A**). To understand the prevalence and heterogeneity of SEZ6 expression, IHC staining from 73 SCLC samples was scored by a pathologist, and the percent

positivity and H-score assessments are summarized in **Fig. 3B** and **Table 2**. About 78% of SCLC tumors had at least 5% of cells positive for SEZ6 with a mean and median percent positivity of 40.4 and 35.0%, respectively (**Fig. 3B**; **Table 2**). The mean and median H-scores for SEZ6 IHC were 66.8 and 55.0, respectively (**Fig. 3B**; **Table 2**). Consistent with RNA expression data, IHC analysis confirms SEZ6 as a prevalent target in SCLC and provides evidence of intratumoral heterogeneity that varies from patient to patient.

In addition to understanding the target prevalence of SEZ6 in SCLC, we sought to understand SEZ6 protein expression in normal human tissues. Multiple samples representing a broad panel of normal human tissues were evaluated by IHC (**Table 3**; **Fig. 3C**). Most tissues surveyed showed no detectable IHC signal, consistent with RNA-seq datasets (**Table 3**; Supplementary Fig. S2C). The tissues with highest staining were cerebellum, cerebrum, spinal cord, and pituitary gland, consistent with RNA-seq data and further establishing SEZ6 as a neuronal and NE marker (**Table 1**; Supplementary Fig. S2C). While the highest expressing tissues are associated with the central nervous system, two highly innervated peripheral tissues, colon and eye, exhibited SEZ6 expression in minor cell populations (**Table 3**; **Fig. 3C**). Specifically, SEZ6 staining was detected in parasympathetic ganglia of the large intestine, in ganglion cells of the retina, and in neurons of the inner and outer plexiform layers of the retina (**Table 3**; **Fig. 3C**). The SEZ6-expressing neurons of the brain, spinal cord, and retina would likely be protected from circulating ADC by the blood-brain and blood-retinal barriers, respectively. Interestingly, while a low level of SEZ6 transcript was detected in adrenal glands by RNA-seq, no protein signal was seen in this tissue. Collectively, the relatively low expression of SEZ6 in normal human tissues makes it an attractive candidate for a calicheamicin-based ADC.

Generation and characterization of mAbs against human SEZ6

To identify a SEZ6 binder for ADC development, we generated murine mAbs against recombinant human SEZ6 using standard hybridoma technology and screened them for SEZ6 binding by ELISA and flow cytometry assays. Sequencing of the hybridoma clones revealed 74 unique SEZ6 antibodies, which were further characterized by surface plasmon resonance (SPR) experiments to determine binding affinity and the kinetic constants (k_{on} and k_{off}). Bio-layer interferometry analysis was used to determine whether the different anti-SEZ6 antibodies compete for SEZ6 binding. Antibodies competing for the same epitope were placed into a single bin, resulting in the identification of seven unique bins. To identify the location of antibody epitopes on SEZ6, we displayed SEZ6 protein fragments on yeast and assessed antibody binding by flow cytometry. At least one binder was identified for each protein domain (Supplementary Fig. S4A). Next, to understand antibody internalization after SEZ6 binding, we employed an indirect killing assay to assess each antibody's ability to mediate saporin-directed cytotoxicity in 293T cells engineered to overexpress full-length human SEZ6. Here, we found that antibodies mediating efficient cell killing were enriched in domains N1, N3, SD1, and SD4 (Supplementary Fig. S4A). A panel of murine antibodies was humanized, and SC17 chosen as the lead based on appropriate properties of the humanized antibody.

To determine reactivity against SEZ6 orthologs, we ectopically expressed human, murine, rat, or cynomolgus monkey (cyno) SEZ6 in 293T cells and generated titration curves for SC17 by flow cytometry. As shown in Supplementary Fig. S4B, SC17 showed minimal binding to SEZ6-negative parental cells but similar binding to 293T cells expressing rat, cyno, and human SEZ6 orthologs with a slight reduction in potency to the murine ortholog based on EC₅₀. SPR

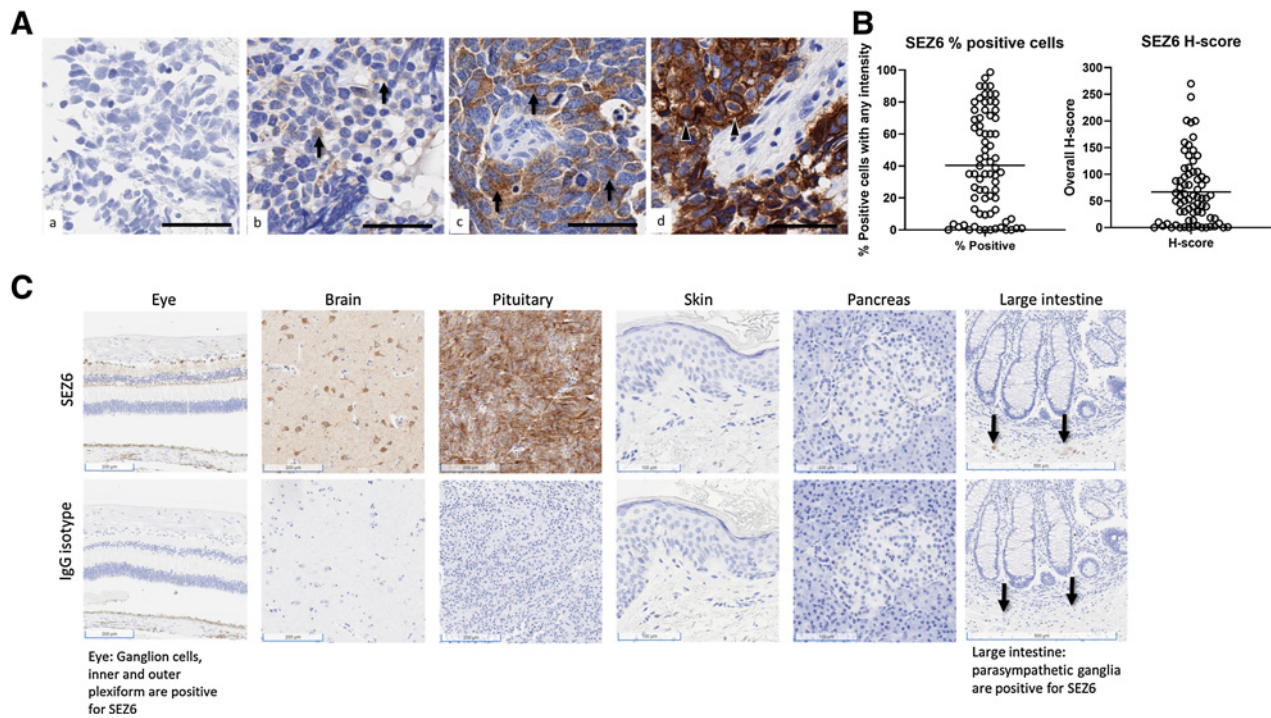


Figure 3. SEZ6 is expressed in primary SCLC samples by IHC. **A**, Representative images of SEZ6 IHC analysis of primary human SCLC tumor samples with a range of target expression (from left to right: seZ6 negative, weakly positive, moderately positive, and strongly positive). Arrows indicate areas of brown SEZ6 staining, with arrow heads indicating specific membranous staining. **B**, Quantitative analysis of percent positivity (left) and H-score (right) across 73 primary human SCLC samples. Scatter plot indicates distribution, and horizontal bar indicates mean. **C**, Representative images of SEZ6 IHC staining across normal human tissues. Arrows indicate staining in parasympathetic ganglia of the large intestine.

revealed binding constants between 2.4 nmol/L for human SEZ6 and 24.9 nmol/L for rat SEZ6 (Supplementary Fig. S4B).

To make an effective ADC, SC17 must bind endogenously expressed SEZ6 and internalize to mediate efficient linker drug delivery. To evaluate SC17 binding to endogenous SEZ6, we used flow cytometry to measure in the H69 SCLC cell line, as well as four SCLC PDX models (Fig. 4A; Supplementary Fig. S4C). Consistent with the IHC data, robust surface staining was detected in parental H69 cells but not in SEZ6 KO H69 (Fig. 4A; Supplementary Fig. S3D). Similar staining intensity was detected in the LU149, LU64, LU95, and LU505 SCLC PDX models (Supplementary Fig. S3F). 293T-SEZ6 and parental 293T cells were included as positive and negative controls, respectively

Table 2. The prevalence of SEZ6 staining across 73 primary human SCLC samples by IHC.

Commercial samples (N = 73)	% positive cells	H-score
25% Percentile	9.73	11.5
Median	35.0	55.0
75% Percentile	70.0	97.5
Range	0–98.7	0–270
(lower, upper 95% CI of mean)	(33.0–47.7)	(52.0–81.5)
Mean	40.4	66.8
SD	31.4	63.2

Note: Percent SEZ6 staining positivity and H-score in primary human SCLC samples.

(Fig. 4A). To assess internalization of the antibody, we performed fluorescence microscopy with SC17 in A549 cells engineered to express human SEZ6 and lysosomal protein LAMP1 fused to mRUBY (red signal in Fig. 4B). We then monitored the cellular localization of the antibody over time. At time 0, SC17 localized to the outer membrane of the cell (green signal in Fig. 4B). After a 4-hour incubation period, we observed strong intracellular staining of SC17 and colocalization with lysosomes (yellow signal in Fig. 4B). Quantitation of the lysosomal colocalization over time revealed rapid internalization of SC17 compared to a CD46-targeted positive control antibody (Fig. 4C). No internalization was observed with a nontargeted IgG1 antibody.

ABBV-011 mediates SEZ6-targeted cytotoxicity in vitro

To generate a SEZ6-targeted ADC, the humanized SC17 mAb was conjugated to the LD19.10 linker drug via site-specific conjugation at a DAR of two (DAR = 2; Fig. 5A). A nontargeted IgG1 antibody was also conjugated to LD19.10 control for nonspecific ADC activity. To confirm that LD19.10 conjugation did not impact the ability of SC17 to bind to SEZ6, we ran flow cytometry analysis on 293T WT cells with or without expression of human, cyno, rat, and murine SEZ6 (Supplementary Fig. S5A). Potency of binding for ABBV-011 was similar to SC17 (Supplementary Figs. S4B, S5A, and S5B).

To test SEZ6-mediated ADC activity, we tested dose-dependent cytotoxicity of ABBV-011, the IgG control ADC, free N-acetyl-γ-calicheamicin, as well as unconjugated SC17 and IgG1 control antibody in 293T cells engineered to express full-length human SEZ6 protein (293T-hSEZ6; Fig. 5B). ABBV-011 elicited target-mediated cell killing in 293T-hSEZ6 cells (IC₅₀ = 75 pmol/L) but not in naïve 293T cells

Table 3. SEZ6 expression in normal tissues by IHC.

Organ	No. of subjects	Positive/negative
Adrenal	11	Negative
Aorta	12	Negative
Appendix	11	Negative
Bladder	8	Negative
Breast	13	Negative
Cerebellum	8	Positive
Cerebrum	10	Positive
Cervix	11	Negative
Colon	49	Positive ^a
Endometrium	9	Negative
Epididymus	12	Negative
Esophagus	11	Negative
Eye	6	Positive ^a
Fallopian tube	11	Negative
Gall bladder	10	Negative
Heart	10	Negative
Kidney	11	Negative
Liver	4	Negative
Lung	11	Negative
Myometrium	11	Negative
Peripheral nerve	14	Negative
Ovary	10	Negative
Pancreas	9	Negative
Parathyroid	4	Negative
Pituitary	15	Positive
Placenta	11	Negative
Prostate	10	Negative
Salivary gland	12	Negative
Skeletal muscle	11	Negative
Skin	11	Negative
Small intestine	11	Negative
Spinal cord	12	Positive
Spleen	9	Negative
Stomach	10	Negative
Testis	11	Negative
Thymus	12	Negative
Thyroid	11	Negative
Tonsil	9	Negative
Trachea	12	Negative
Ureter	7	Negative
Vas deferens	11	Negative

Note: Panel of human tissues stained for SEZ6 by IHC. Number of unique samples tested for each organ and staining outcome is summarized in columns 2 and 3, respectively.

^aIndicates staining was seen only in the neuronal cells of these tissues.

($IC_{50} > 100$ nmol/L), where both ABBV-011 and the control ADC had similar unspecific activity at high nanomolar concentrations (Fig. 5B; Supplementary Fig. S5C). The free warhead N-acetyl- γ -calicheamicin was active in both 293T-expressing human SEZ6 ($IC_{50} = 112$ pmol/L) and naïve 293T ($IC_{50} = 111$ pmol/L), whereas both unconjugated antibodies had no activity at the highest concentration tested (100 nmol/L, Fig. 5B; Supplementary Fig. S5C). We similarly ran cytotoxicity assays for 293T expressing cyno, mouse, and rat SEZ6. Consistent with the cross-species binding seen by flow cytometry for SC17, ABBV-011 was able to induce potent killing against cyno, rat, and murine SEZ6 (Supplementary Fig. S5B).

Next, we turned to human SCLC cell lines with endogenous expression of SEZ6. Here, we compared ABBV-011 activity in NCI-H69 with and without SEZ6 KO. ABBV-011 ($IC_{50} = 106$ pmol/L) but not the

control ADC ($IC_{50} \sim 50$ nmol/L) had strong activity in parental NCI-H69 cells (Fig. 5C). In NCI-H69 cells with SEZ6 KO, ABBV-011 had no activity at the highest concentration tested (100 nmol/L). We conclude that ABBV-011 mediates target-specific cytotoxicity in SEZ6-positive cells *in vitro*.

ABBV-011 is efficacious in PDX models of SCLC

To confirm dose linearity of ABBV-011 in mice, pharmacokinetic studies were run in naïve animals following a single dose. Between 0.5 and 8 mg/kg, ABBV-011 exposures exhibited a linear, dose-dependent effect on plasma exposure, and the clearance rates were similar to those observed for other ADCs in mouse (Supplementary Fig. S6A, left; ref. 34). In addition, to understand ABBV-011 stability *in vivo*, we measured the total antibody and ADC concentrations for 1 mg/kg ABBV-011 in tumor bearing mice over 14 days (Supplementary Fig. S6A, right). The concentration of total antibody and ADC remained similar and stable over 14 days, indicating the noncleavable disulfide linker of ABBV-011 is stable in circulation.

We next tested the antitumor activity of ABBV-011 using PDX models of SCLC which were derived from well annotated primary human tumors and previously characterized for *in vivo* growth kinetics and chemotherapy sensitivity (20). A single dose of ABBV-011 resulted in significant, and dose-dependent tumor regression in LU64, a SEZ6-positive PDX line (Fig. 6A; Supplementary Fig. S3F). Treatment with vehicle, nontargeting antibody, SC17, or nontargeting antibody conjugated to LD19.10 had no significant impact on tumor growth. While 2 mg/kg ABBV-011 was sufficient to induce sustained tumor regression, a molar equivalent dose of free NAC-LD19.10 had minimal effect, suggesting that the ADC can significantly enhance tumoral exposure to the cytotoxic payload (Fig. 6A). Notably, a single cycle of cisplatin and etoposide, standard-of-care chemotherapy in SCLC, showed less sustained tumor regression than the 0.5 mg/kg dose of ABBV-011. Robust, dose-dependent tumor regression was also observed in two additional SEZ6-positive PDX, LU95 and LU149, albeit with slightly lower potency (Fig. 6B and C; Supplementary Fig. S3F). Similar efficacy results were observed when ABBV-011 was tested across a panel of 7 SEZ6-positive PDX, and outperformed cisplatin/etoposide in all cases (Fig. 6A–C; Supplementary Fig. S6B). Notably, ABBV-011 remained active in LU129, a model with 60% SEZ6 positivity, suggesting ABBV-011 could be effective in tumor with intermediate expression. To evaluate the target dependency of ABBV-011, an efficacy study was run in LU505, a SCLC PDX with minimal SEZ6 expression (Supplementary Fig. S3F; Fig. 4A). Although a CD46.LD19.10 ADC and cisplatin/etoposide caused LU505 tumor regression, ABBV-011 had minimal effect on tumor growth even at an 8 mg/kg dose (Fig. 6D). These data suggest that ABBV-011 requires SEZ6 expression to induce antitumor activity *in vivo*, consistent with the *in vitro* studies (Fig. 6D; Fig. 5C).

Discussion

SCLCs represent a small (10%–15%) yet highly aggressive subgroup of lung cancers with a median 5-year survival of about 7% and lack of actionable driver mutations (35). SCLC are thought to develop from a NE cell of origin and have near-universal inactivation of the TP53 and RB1 tumor suppressor pathways, as well as genomic amplification and overexpression of MYC, resulting in rampant growth and genomic instability (36). Because of the aggressive nature of the disease, the majority of SCLC cases are diagnosed after the tumor metastasizes to other organs (extensive stage). Platinum-based chemotherapy in

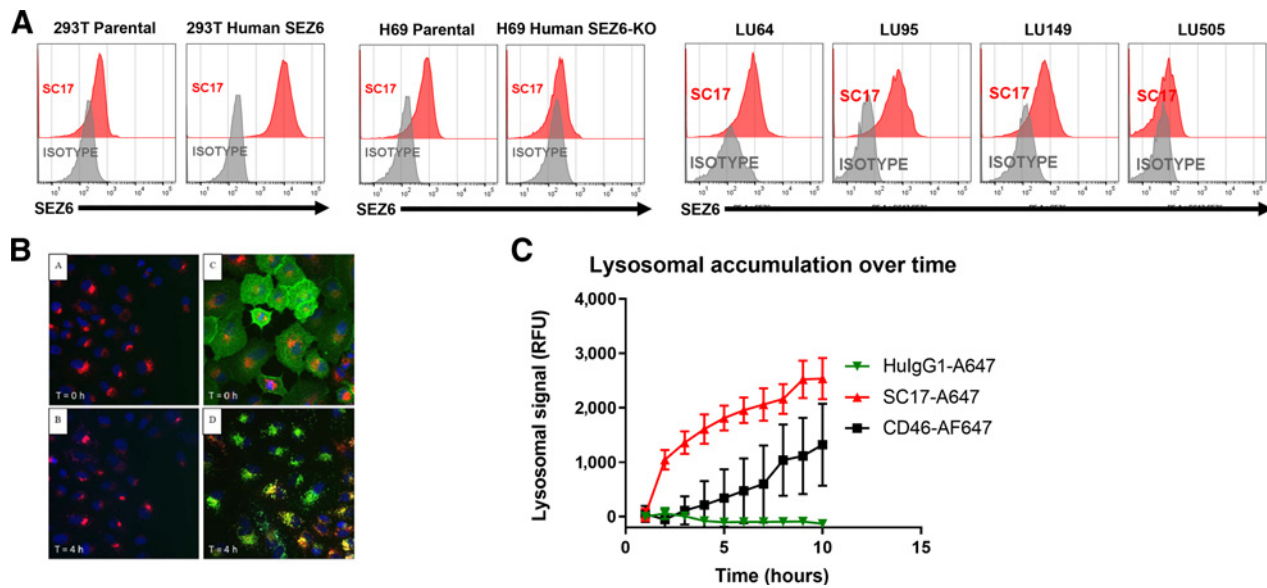


Figure 4. SC17 is a SEZ6-specific antibody that internalizes when bound to SEZ6 on the surface of SCLC cells. **A**, Parental 293T and 293T cells overexpressing human SEZ6, H69 cells and SEZ6 KO H69 cells, and SCLC PDX models, LU149, LU64, LU95, and LU505, were stained with SC17 or control IgG antibody conjugated to the fluorophore PE. Specific SEZ6 cell surface staining is observed with SC17-PE but not with IgG-PE in 293T cells overexpressing SEZ6, in naïve H69 cells, and in the two SCLC PDX models. **B**, Time course fluorescence microscopy with SC17-A647 in A549 cells engineered to express human SEZ6 and lysosomal protein LAMP1 fused to mRUBY (red signal). At time 0, SC17 localized to the outer membrane of the cell (green signal). After a 4-hour incubation period, we observed strong intracellular staining of SC17-A647 and colocalization with lysosomes (yellow signal). **C**, Time course quantitation of the lysosomal colocalization of SC17-A647 compared with CD46-A647 and IgG-A647 (negative control).

combination with etoposide and immune checkpoint inhibitors temporarily controls disease progression in most patients, but virtually all extensive stage SCLC eventually recur and become resistant to standard-of-care chemotherapy, thus highlighting the need for novel therapeutic options.

Because of the initially chemosensitive nature of SCLC, we hypothesized that recurrent SCLC may be susceptible to DNA-damaging agents other than platinum, such as calicheamicin. Calicheamicin is one of the most potent naturally occurring cytotoxic agents with a mechanism of action that involves interaction with the minor groove

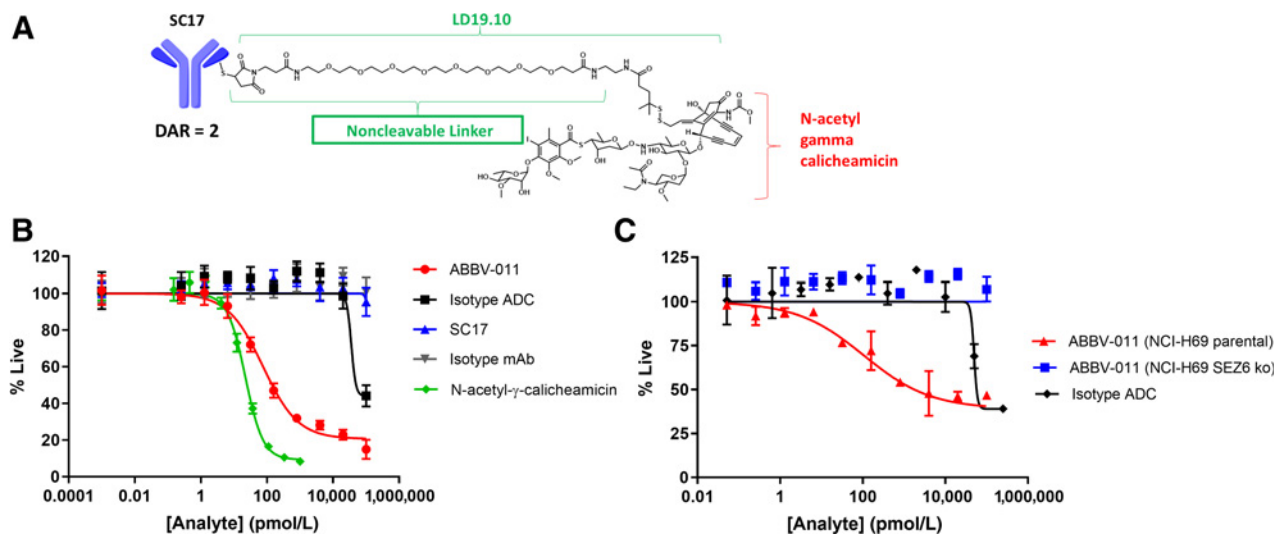


Figure 5. ABBV-011 potently and selectively kills SEZ6-positive cells *in vitro*. **A**, Schematic depiction of the ABBV-011 ADC. ABBV-011 consists of mAb SC17 conjugated to two molecules of LD19.10 linker drug (DAR2). **B**, 293T-SEZ6 cells were exposed to increasing concentrations of ABBV-011, nontargeted control ADC, unconjugated SC17 antibody targeting SEZ6, a nontargeted control antibody, or free calicheamicin. Percentage of live cells was determined by a luminometric viability assay. **C**, Parental NCI-H69 cells and SEZ6-KO NCI-H69 cells were exposed to increasing concentrations of ABBV-011 or nontargeted control ADC. Percentage of live cells was determined by a luminometric viability assay.

multiple PDX undergoing complete regression after a single dose (Fig. 6). This result is in line with the proposed mechanism of action for ABBV-011, which requires internalization of the ABBV-011-SEZ6 complex, followed by cleavage of the ADC linker in lysosomes and release of active calicheamicin payload (Supplementary Fig. S7). In contrast to other calicheamicin ADC, such as Mylotarg and Besponsa, the ABBV-011 linker lacks the acid labile diamide group, and, consequently, does not result in any detectable DMH metabolites when dosed in rat or monkey at levels above the therapeutic dose (Table 1). In line with the observed changes in ADC metabolism, the therapeutic index, as calculated by murine efficacy and monkey toxicology, was significantly improved for ABBV-011 compared with ADCs with the same antibody and same payload conjugated via a cleavable linker (22). Importantly, ABBV-011 demonstrated preclinical efficacy in PDX models with a range of platin sensitivity. Taken together, ABBV-011 is a novel calicheamicin-based ADC for the treatment of SCLC that is currently being tested in a phase I clinical trial.

Authors' Disclosures

W.R. Wiedemeyer reports personal fees from AbbVie, Inc. during the conduct of the study; and personal fees from AbbVie, Inc. outside the submitted work. A. Schammel reports personal fees from AbbVie, Inc. outside the submitted work; in addition, A. Schammel has a patent for WO2019232241 A1 issued. X. Zhao reports personal fees from AbbVie, Inc. outside the submitted work. H. Sarvaiya reports personal fees from AbbVie, Inc. outside the submitted work. M. Pysz reports personal fees from AbbVie, Inc. during the conduct of the study. M. You reports personal fees from AbbVie, Inc. during the conduct of the study; and personal fees from AbbVie, Inc. outside the submitted work. K. Isse reports personal fees from AbbVie, Inc. during the conduct of the study. D. French reports other support from AbbVie, Inc. outside the submitted work. A.T. Dang reports personal fees from AbbVie, Inc. during

the conduct of the study; and personal fees from AbbVie, Inc. outside the submitted work. Z. Zhang reports personal fees from AbbVie, Inc. during the conduct of the study; and personal fees from AbbVie, Inc. outside the submitted work. M. Aujay reports personal fees from AbbVie, Inc. outside the submitted work. A.J. Bankovich reports personal fees from AbbVie, Inc. during the conduct of the study. P. Vitorino reports personal fees from AbbVie, Inc. during the conduct of the study. No disclosures were reported by the other authors.

Authors' Contributions

W.R. Wiedemeyer: Supervision, methodology, writing–review and editing. J. Gavrilyuk: Conceptualization, supervision, methodology. A. Schammel: Investigation, methodology. X. Zhao: Data curation, visualization. H. Sarvaiya: Methodology. M. Pysz: Investigation, methodology, writing–review and editing. C. Gu: Investigation. M. You: Methodology. K. Isse: Investigation. T. Sullivan: Investigation. D. French: Formal analysis. C. Lee: Investigation. A.T. Dang: Investigation. Z. Zhang: Investigation. M. Aujay: Conceptualization, formal analysis, supervision. A.J. Bankovich: Conceptualization. P. Vitorino: Conceptualization, formal analysis, supervision, writing–original draft, writing–review and editing.

Acknowledgments

The authors would like to thank Nicole Taylor (former AbbVie employee) for pharmacokinetic analyses, and Elmer Payson (AbbVie employee) for animal work.

The costs of publication of this article were defrayed in part by the payment of page charges. This article must therefore be hereby marked *advertisement* in accordance with 18 U.S.C. Section 1734 solely to indicate this fact.

Received October 20, 2021; revised January 24, 2022; accepted March 4, 2022; published online June 1, 2022.

References

- Lee M, Ellestad GA, Borders DB. Calicheamicins: discovery, structure, chemistry, and interaction with DNA. *Acc Chem Res* 1991;24:8:235–43.
- Nicolaou KC, Rigol S. The role of organic synthesis in the emergence and development of antibody–drug conjugates as targeted cancer therapies. *Angew Chem Int Ed Engl* 2019;58:11206–41.
- Appelbaum FR, Bernstein ID. Gemtuzumab ozogamicin for acute myeloid leukemia. *Blood* 2017;130:2373–6.
- Hamann PR, Hinman LM, Hollander I, Beyer CF, Lindh D, Holcomb R, et al. Gemtuzumab ozogamicin, a potent and selective anti-CD33 antibody–calicheamicin conjugate for treatment of acute myeloid leukemia. *Bioconjug Chem* 2002;13:47–58.
- Dowell JA, Korh-Bradley J, Liu H, King SP, Berger MS. Pharmacokinetics of gemtuzumab ozogamicin, an antibody-targeted chemotherapy agent for the treatment of patients with acute myeloid leukemia in first relapse. *J Clin Pharmacol* 2001;41:1206–14.
- Giles FJ, Kantarjian HM, Kornblau SM, Thomas DA, Garcia-Manero G, Waddelow TA, et al. Mylotarg (gemtuzumab ozogamicin) therapy is associated with hepatic venoocclusive disease in patients who have not received stem cell transplantation. *Cancer* 2001;92:406–13.
- Garrido-Laguna I, Krop I, Burris HA 3rd, Hamilton E, Braiteh F, Weise AM, et al. First-in-human, phase I study of PF-06647263, an anti-EFNA4 calicheamicin antibody–drug conjugate, in patients with advanced solid tumors. *Int J Cancer* 2019;145:1798–808.
- Epenetos AA, Snook D, Durbin H, Johnson PM, Taylor-Papadimitriou J. Limitations of radiolabeled monoclonal antibodies for localization of human neoplasms. *Cancer Res* 1986;46:3183–91.
- Rekhtman N. Neuroendocrine tumors of the lung: an update. *Arch Pathol Lab Med* 2010;134:1628–38.
- Foster NR, Qi Y, Shi Q, Krook JE, Kugler JW, Jett JR, et al. Tumor response and progression-free survival as potential surrogate endpoints for overall survival in extensive stage small-cell lung cancer: findings on the basis of North Central Cancer Treatment Group trials. *Cancer* 2011;117:1262–71.
- Augustyn A, Borromeo M, Wang T, Fujimoto J, Shao C, Dospoy PD, et al. ASCL1 is a lineage oncogene providing therapeutic targets for high-grade neuroendocrine lung cancers. *Proc Natl Acad Sci U S A* 2014;111:14788–93.
- Kasprzak A, Zabel M, Biczysko W. Selected markers (chromogranin A, neuron-specific enolase, synaptophysin, protein gene product 9.5) in diagnosis and prognosis of neuroendocrine pulmonary tumours. *Pol J Pathol* 2007;58:23–33.
- Jensen SM, Gazdar AF, Cuttitta F, Russell EK, Linnoila RI. A comparison of synaptophysin, chromogranin, and L-dopa decarboxylase as markers for neuroendocrine differentiation in lung cancer cell lines. *Cancer Res* 1990;50:6068–74.
- Irizarry RA, Hobbs B, Collin F, Beazer-Barclay YD, Antonellis KJ, Scherf U, et al. Exploration, normalization, and summaries of high density oligonucleotide array probe level data. *Biostatistics* 2003;4:249–64.
- George J, Lim JS, Jang SJ, Cun Y, Ozretic L, Kong G, et al. Comprehensive genomic profiles of small cell lung cancer. *Nature* 2015;524:47–53.
- Jiang L, Huang J, Higgs BW, Hu Z, Xiao Z, Yao X, et al. Genomic landscape survey identifies SRSF1 as a key oncogene in small cell lung cancer. *PLoS Genet* 2016;12:e1005895.
- Clinical Lung Cancer Genome Project, Network Genomic Medicine. A genomics-based classification of human lung tumors. *Sci Transl Med* 2013;5:209ra153.
- Team RC. R: A language and environment for statistical computing. Vienna, Austria: R Foundation for Statistical Computing; 2013.
- Diehl KH, Hull R, Morton D, Pfister R, Rabemampianina Y, Smith D, et al. A good practice guide to the administration of substances and removal of blood, including routes and volumes. *J Appl Toxicol* 2001;21:15–23.
- Anderson WC, Boyd MB, Aguilar J, Pickell B, Laysang A, Pysz MA, et al. Initiation and characterization of small cell lung cancer patient-derived xenografts from ultrasound-guided transbronchial needle aspirates. *PLoS One* 2015;10:e0125255.
- AbbVie Stemcentrx LLC, assignee. Anti-Sez6 antibody drug conjugates and methods of use patent WO/2019/232241; 2019.
- AbbVie Stemcentrx LLC, assignee. Anti-Sez6 antibody drug conjugates and methods of use; 2021.

23. Larson RA, Sievers EL, Stadtmauer EA, Lowenberg B, Estey EH, Dombret H, et al. Final report of the efficacy and safety of gemtuzumab ozogamicin (Mylotarg) in patients with CD33-positive acute myeloid leukemia in first recurrence. *Cancer* 2005;104:1442–52.
24. Yurkiewicz IR, Muffly L, Liedtke M. Inotuzumab ozogamicin: a CD22 mAb-drug conjugate for adult relapsed or refractory B-cell precursor acute lymphoblastic leukemia. *Drug Des Devel Ther* 2018;12:2293–300.
25. Beck A, Goetsch L, Dumontet C, Corvaia N. Strategies and challenges for the next generation of antibody-drug conjugates. *Nat Rev Drug Discov* 2017;16:315–37.
26. Elvington M, Liszewski MK, Atkinson JP. CD46 and oncologic interactions: Friendly fire against cancer. *Antibodies* 2020;9:59.
27. Eichhorn JH, Lawrence WD, Young RH, Scully RE. Ovarian neuroendocrine carcinomas of non-small-cell type associated with surface epithelial adenocarcinomas. A study of five cases and review of the literature. *Int J Gynecol Pathol* 1996;15:303–14.
28. Travis WD, Linnoila RI, Tsokos MG, Hitchcock CL, Cutler GB Jr, Nieman L, et al. Neuroendocrine tumors of the lung with proposed criteria for large-cell neuroendocrine carcinoma. An ultrastructural, immunohistochemical, and flow cytometric study of 35 cases. *Am J Surg Pathol* 1991;15:529–53.
29. Shimizu-Nishikawa K, Kajiwara K, Sugaya E. Cloning and characterization of seizure-related gene, SEZ-6. *Biochem Biophys Res Commun* 1995;216:382–9.
30. Gunnerson JM, Kim MH, Fuller SJ, De Silva M, Britto JM, Hammond VE, et al. Sez-6 proteins affect dendritic arborization patterns and excitability of cortical pyramidal neurons. *Neuron* 2007;56:621–39.
31. Kudoh S, Tenjin Y, Kameyama H, Ichimura T, Yamada T, Matsuo A, et al. Significance of achaete-scute complex homologue 1 (ASCL1) in pulmonary neuroendocrine carcinomas; RNA sequence analyses using small cell lung cancer cells and Ascl1-induced pulmonary neuroendocrine carcinoma cells. *Histochem Cell Biol* 2020;153:443–56.
32. Rudin CM, Poirier JT, Byers LA, Dive C, Dowlati A, George J, et al. Molecular subtypes of small cell lung cancer: a synthesis of human and mouse model data. *Nat Rev Cancer* 2019;19:289–97.
33. Piloni M, Hsia HE, Hartmann J, Rudan Njavro J, Shmueli MD, Muller SA, et al. Seizure protein 6 controls glycosylation and trafficking of kainate receptor subunits GluK2 and GluK3. *EMBO J* 2020;39:e103457.
34. Okamoto H, Oitate M, Hagihara K, Shiozawa H, Furuta Y, Ogitani Y, et al. Pharmacokinetics of trastuzumab deruxtecan (T-DXd), a novel anti-HER2 antibody-drug conjugate, in HER2-positive tumour-bearing mice. *Xenobiotica* 2020;50:1242–50.
35. Gazdar AF, Bunn PA, Minna JD. Small-cell lung cancer: what we know, what we need to know and the path forward. *Nat Rev Cancer* 2017;17:765.
36. Ireland AS, Micinski AM, Kastner DW, Guo B, Wait SJ, Spainhower KB, et al. MYC drives temporal evolution of small cell lung cancer subtypes by reprogramming neuroendocrine fate. *Cancer Cell* 2020;38:60–78.
37. Walker S, Landovitz R, Ding WD, Ellestad GA, Kahne D. Cleavage behavior of calicheamicin gamma 1 and calicheamicin T. *Proc Natl Acad Sci U S A* 1992;89:4608–12.
38. Tang CH, Parham C, Shocron E, McMahon G, Patel N. Picoplatin overcomes resistance to cell toxicity in small-cell lung cancer cells previously treated with cisplatin and carboplatin. *Cancer Chemother Pharmacol* 2011;67:1389–400.